ACS OMEGA

Open Access

http://pubs.acs.org/journal/acsodf

Article

Low-Cost Preparation of Diamond Nanopillar Arrays Based on Polystyrene Spheres

Xin Tan,* Zhanqing He, Wenbin Li, Qiao Yang, Jian Wang, Lei Cang, Yanlong Du, and Hui Qi

Cite This: *ACS Omega* 2024, 9, 27492−27498

Read Online

ACCESS | Metrics & More | Article Recommendations

ABSTRACT: Diamond nanopillar arrays can enhance the fluorescence collection of diamond color centers, playing a crucial role in quantum communication and quantum sensing. In this paper, the preparation of diamond nanopillar arrays was realized by the processes of polystyrene (PS) sphere array film preparation, PS sphere etching shrinkage control, tilted magnetron sputtering of copper film, and oxygen plasma etching. Closely aligned PS sphere array films were prepared on the diamond surface by the gas−liquid interfacial method, and the effects of ethanol and dodecamethylacrylic acid solutions on the formation of the array films were discussed. Controllable reduction of PS sphere diameter is realized by the oxygen plasma etching process, and the changes of the PS sphere array film under the influence of etching power, bias power, and etching time are discussed. Copper antietching films were prepared at the top of arrayed PS spheres by the tilted magnetron sputtering method, and the antietching effect of copper films with different thicknesses was explored. Diamond nanopillar arrays were prepared by oxygen plasma etching, and the effects of etching under different process parameters were discussed. The prepared diamond nanopillars were in hexagonal close-rowed arrays with a spacing of 800 nm and an average diameter of 404 nm, and the spacing, diameter, and height could be parametrically regulated. Raman spectroscopy and photoluminescence spectroscopy detection revealed that the prepared diamond nanopillar array still maintains polycrystalline diamond properties, with only a small amount of the graphite phase appearing. Moreover, the prepared diamond nanopillar array can enhance the photoluminescence of diamond color centers by approximately 2 times. The fabrication method of diamond nanopillar array structures described in this article lays the foundation for quantum sensing technology based on diamond nanostructures.

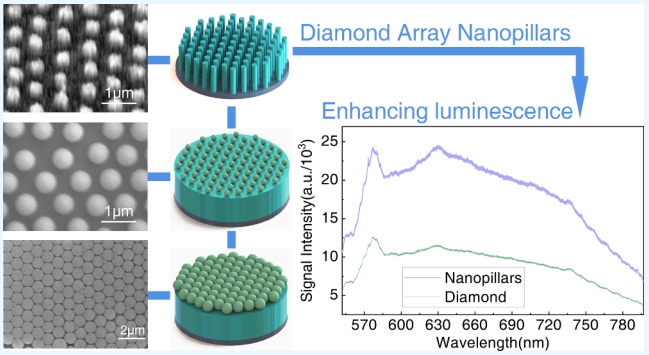

1. INTRODUCTION

With the properties of stable luminescence at room temperature, high brightness, long spin coherence time, and controllable magnetic resonance of the ground state, diamond NV color centers are a more stable single-photon source at room temperature and have a wide range of applications in the fields of quantum information technology, nanosensors, and biofluorescence labeling.[1−4] However, due to the large refractive index gradient at the interface between diamond and air, most of the photons emitted from the color center are fully reflected back to the substrate and cannot be effectively collected, which seriously hampers its development in areas such as single-photon sources and nanosensing.

It has been found that the collection of color-centered photons can be enhanced by the generation of confined light fields or swift fields from diamond nanocrystals,[5] nanopillars,[6−9] or metal nanostructures,[10−12] among others. For example, Babinec et al.[13] showed that diamond nanowires with a diameter of 200 nm and a length of 2 μm can improve the transmittance of photons emitted from NV color centers by nearly an order of magnitude compared to diamond masses.

There are two main methods for the preparation of nanopillars: top-down and bottom-up. Among them, bottom-up mainly employs customized templates to achieve the limitation of nanopillar size and then controllable growth of diamond within the template by chemical vapor deposition and other methods.[14] The diamond grain boundaries and graphite phases prepared by such methods are biased, which increases the scattering of photons and is not conducive to improving the collection efficiency of emitted photons.[15] Top-down approaches have focused on forming nanopillar structures by etching diamond blocks or diamond films, but there has not been a cost-versus-quality solution for the preparation of etch masks. Most of the nanopillar etching masks are currently

Received: March 18, 2024
Revised: May 3, 2024
Accepted: June 4, 2024
Published: June 12, 2024

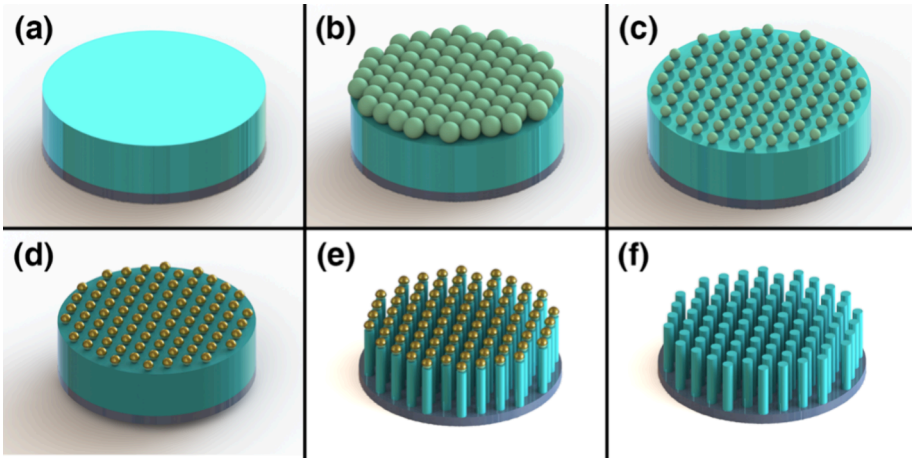

Figure 1. Process flow of diamond nanopillar array preparation (a) growing a diamond film on a silicon substrate, (b) preparing an hexagonal densely arranged PS ball film on the surface of the diamond film, (c) oxygen etching to control the uniform shrinkage of PS balls, (d) tilted magnetron sputtering of the Cu antietch layer, (e) oxygen etching of the diamond film to prepare the nanopillar arrays, and (f) diamond nanopillar arrays obtained after concentrated hydrochloric acid washing.

prepared by electron beam lithography (EBL) technique.[16,17] Ali Momenzadeh et al.[3] prepared a tapered diamond nanopillar array using EBL and found that this tapered nanopillar can effectively increase the photon collection efficiency by more than 10 times. Although this technique enables the preparation of nanoscale-sized etch mask arrays,[18,19] its high fabrication cost makes the technique difficult to be widely used. In contrast, another cost-effective and efficient method for mask preparation involves the self-assembly process of metal or nonmetallic spheres.[20−22] Researchers such as Li and Hatta,[23] Babchenko et al.,[24] Smirnov et al.,[25] and Janssen and Gheeraert[26] have achieved patterned masks through the dewetting of aluminum, nickel, and gold films. However, controlling the diameter of these masks proves challenging, resulting in the fabrication of diamond nanowires with diameters typically in the range of a few tens of nanometers. Domonkos and Kromka,[27] on the other hand, have demonstrated the formation of well-ordered array films through the self-assembly of polystyrene (PS) spheres. Unfortunately, the low etch resistance of PS spheres makes them unsuitable as etching masks for diamond.

In this study, a diamond film is used as the substrate for the controllable preparation of PS ball monolayer array membrane structures. The controllable reduction of the PS sphere diameter was realized by controlling the etching parameters. Tilted sputtering of the copper antietching layer to increase the PS sphere array mask capability and oxygen plasma etching were used to prepare diamond array nanopillars.

2. MATERIALS AND METHODS

The preparation process of diamond array nanopillars proposed in this paper is shown in Figure 1. The starting material is a single-sided (001) polished monocrystalline silicon substrate, on which a micrometer-thick diamond film is first grown. Next, PS ball array monolayers were prepared on the diamond film surface. The PS ball size reduction is then controlled by oxygen plasma etching. The copper resist etching layer is then sputtered onto the surface of the PS ball by tilted magnetron sputtering. Finally, diamond array nanopillars were prepared by oxygen plasma etching under an etching mask. Arrayed diamond nanopillars were obtained after being cleaned with concentrated hydrochloric acid.

2.1. Diamond Film Preparation. A single-sided polished (001) silicon wafer (2 cm × 2 cm) was employed as the substrate for diamond growth. The substrate was ultrasonically oscillated in a diamond suspension for 40 min to achieve a nucleation density of 1×10^9 cm^{-2}.[28,29] Subsequently, excess suspension was sequentially removed by washing with alcohol and deionized water followed by drying with nitrogen gas. Diamond growth took place in a microwave plasma chemical vapor deposition (MPCVD) system using a gas mixture of 1:100 CH_4:H_2. The growth rate was approximately 500 nm/h, and the surface roughness was around 20 nm. The deposition temperature was approximately 900 °C, the operating pressure was about 4000 Pa, and the deposition time was 3 h.

2.2. PS Ball Self-Assembled Monolayer Membrane Preparation. The diamond substrate was sequentially sonicated in acetone, alcohol, and deionized water for 10 min to remove surface impurities and blown dry with nitrogen. Anhydrous ethanol was mixed with PS ball suspension (cat. no.: YG1200; diam: 800 nm; BC%: 2.5%) in a ratio of 4:1 and sonicated for 10 min to make the PS ball dispersion uniform. A glass plate tilted at 20° was placed on the surface of deionized water, and a drop of PS/ethanol mixture was added to the glass plate so that it was slowly scratched into the gas−liquid interface; it was left to stand for 10 min so that the PS spheres were dispersed and distributed on the interface. A dodecamethyl methacrylic acid (SDS) solution was added dropwise to the glass so that it was slowly scratched into the interface and again left for 10 min to allow the PS spheres to self-assemble into an array monolayer. The substrate was placed in deionized water in the absence of the PS ball monolayer and slowly fished out from underneath the PS ball monolayer at a 5° angle of inclination. The samples with the PS ball monolayer were dried in a constant temperature oven for 20 min to allow the PS ball layer to physically adsorb onto the surface of the diamond film.

2.3. PS Ball Controllable Shrinkage. The process was completed in an inductively coupled plasma etching machine (ICP) using oxygen plasma etching at an oxygen flow rate of 50 sccm and an etching pressure of 2 Pa. Etching powers were selected as 200, 300, and 400 W, bias powers were selected as 0 20, and 50 W, and etching times were selected as 0.5, 1, 2, 3, and 4 min.

https://doi.org/10.1021/acsomega.4c02618
ACS Omega 2024, 9, 27492−27498

2.4. Preparation of the Etch-Resistant Mask. Due to the high etch selectivity of diamond under copper masking, a copper metal layer was employed for etch-resistant mask preparation.[28,30] The deposition of the copper film was conducted in a physical vapor deposition (PVD) system using a 2.36 in. copper target with a purity of 99.999%. The sputtering power was set at 40 W, with a substrate-to-target angle of 30°, a distance of 260 mm, a working pressure of 1 Pa, and an argon flow rate of 25 sccm. The deposition rate of the copper film was 0.08 nm/s (estimated by deposition of the film thickness for 1 h).

2.5. Diamond Nanopillar Array Etching. The process was done in an inductively coupled plasma etching machine (ICP) with oxygen plasma etching, an oxygen flow rate of 50 sccm, an etching pressure of 2 Pa, etching powers of 200, 300, and 400 W, bias powers of 0, 20, and 50 W, and etching times of 5, 10, 15, 20, and 40 min. After preparation of diamond nanopillars, PS spheres and Cu membranes were removed by means of concentrated hydrochloric acid dissolution and washed with anhydrous ethanol, acetone, and deionized water accordingly.

2.6. Characterization. Morphological characterization was performed using scanning electron microscopy (SEM, TESCAN MIRA4) at a tilted 45° or 90° overhead view. The surface roughness was characterized using atomic force microscopy (AFM, Dimension Edge, Bruker). The characterization of crystal properties and optical performance was conducted by using a Raman-fluorescence confocal microscope (Horiba LabRam HR Evolution). Continuous-wave laser excitation at a wavelength of 532 nm was employed for the analysis.

3. RESULTS AND DISCUSSION

PS ball self-assembled monolayers were prepared by a gas−liquid interfacial method and transferred to the diamond surface by substrate salvage. A comparison of anhydrous ethanol and SDS solution before and after addition is shown in Figure 2. As shown in Figure 2a, the monolayer membrane was

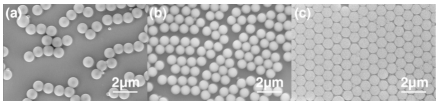

Figure 2. Preparation of PS ball monolayers under different conditions: (a) PS ball aqueous solution, (b) PS ball/ethanol mixture, and (c) PS ball/ethanol mixture with dropwise addition of SDS solution.

prepared by direct dropwise addition of an aqueous solution of PS ball suspension into deionized water and fished out. The PS balls were mostly distributed in whiskers, failing to form a large area of close arrangement, with only a few individual PS ball clustering phenomenon. As shown in Figure 2b, the monolayer film was prepared by fishing out the PS ball/ethanol mixture directly after dropwise addition; at this time, most of the PS balls are tightly stacked and show short range-ordered-like distribution. Comparison of the case without ethanol addition can be analyzed to know that ethanol plays a key role in the agglomeration of PS. As shown in Figure 2c for the PS ball/ethanol mixture added dropwise followed by an SDS solution and fished out of the prepared monolayer film, at this time, the PS spheres are arranged tightly on the diamond surface and are long range-ordered, indicating that the SDS solution plays a key role in the tight arrangement of the PS spheres.

To prepare array etching masks with different diameters at the same pitch, in this paper, the PS ball monolayer film is etched by the oxygen plasma etching method, and the PS ball size is realized by controlling the etching power, bias power, and etching time, as shown in Figure 3. In comparison to

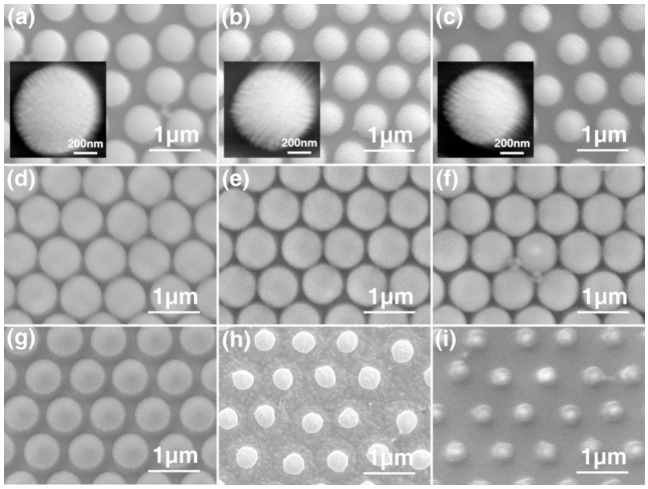

Figure 3. PS ball shrinkage control with different etching parameters. The etching power, bias power, and etching time are (a) 200 W, 50 W, and 1 min, (b) 300 W, 50 W, and 1 min, (c) 400 W, 50 W, and 1 min, (d) 300 W, 0 W, and 1 min, (e) 300 W, 20 W, and 1 min, (f) 300 W, 20 W, and 0.5 min, (g) 300 W, 20 W, and 2 min, (h) 300 W, 20 W, and 3 min, and (i) 300 W, 20 W, and 4 min, respectively.

Figure 3a−c, under the conditions of maintaining a bias power of 50 W and an etching time of 1 min unchanged, the etching powers of 200, 300, and 400 W, respectively, show no significant impact on the periodic array of PS spheres. At an etching power of 200 W, the average diameter of the PS ball shrinks to 694 nm, with a shrinkage rate of 106 nm/min, and the surface of the ball is relatively smooth. When the etching power is 300 W, the average diameter of the PS ball shrinks to 651 nm, the shrinkage rate is 149 nm/min, and the surface roughness of the ball has a corresponding increase. When the etching power is 400 W, the average diameter of the PS ball shrinks to 596 nm, the shrinkage rate is 204 nm/min, the surface roughness of the ball increases again, and the flocculent structure appears at the edge (as it can be seen on SEM images). The adjustment of the etching power can realize the PS ball diameter reduction rate control, but the larger the etching power on the PS ball, the more serious the surface damage is. Considering the roughness and etching rate, the etching power is 300 W.

Comparing Figure 3b,d,e, under the constant etching power of 300 W and the etching time of 1 min, we examine the effects of different bias powers (0, 20, and 50 W) on the etching of PS spheres. The gap between the PS balls changes insignificantly when the bias power is 0 W. When the bias power is 20 W, there is a gap between the PS balls, and the average diameter of the PS balls is 781 nm with a shrinkage rate of 19 nm/min. Compared to the bias power of 50 W, the surface roughness of the PS ball is small, and the bias power is chosen to be 20 W. Comparing Figure 3e−i, with the etching power held constant at 300 W and the bias power at 20 W, we examine the etching of PS spheres under different etching times (1, 2, 3, and 4

https://doi.org/10.1021/acsomega.4c02618
ACS Omega 2024, 9, 27492−27498

min). The periodic array of PS spheres shows no significant change with increasing etching time, but the average diameter of PS spheres gradually decreases. The average diameters of PS spheres under etching for 0.5, 1, 2, 3, and 4 min were 792, 781, 679, 408, and 375 nm, respectively.

The PS ball antietching ability is weaker than diamond and cannot be used directly as an etching mask, so the use of a sputtering copper film on the surface of the PS ball improves its antietching ability.[31,32] Based on the PS array with an average diameter of 408 nm (as shown in Figure 3h), Cu films were deposited on top of the PS spheres by using magnetron sputtering. Deposition was performed at an angle, with deposition times of 10, 20, 30, 40, 50, and 60 s, resulting in Cu film thicknesses of 8, 16, 24, 32, 40, and 48 nm, respectively, forming copper antietching masks. The etching resistance of various thicknesses of the Cu film was assessed through oxygen etching following the deposition of the Cu film with the etching power set at 300 W, bias power at 50 W, and etching time at 10 min, as illustrated in Figure 4. When the Cu

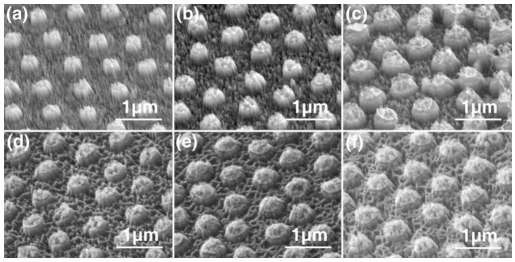

Figure 4. Etch resistance effect of different thicknesses of copper films: (a) 8, (b) 16, (c) 24, (d) 32, (e) 40, and (f) 48 nm.

film is 8 nm, the PS sphere is disrupted and the diamond nanopillar consists of multiple finer nanopillars with dense nanopins present in the interstices of the nanopillars. When the Cu film is 16 nm, the oxygen plasma is less destructive to the PS spheres, but the periphery of the nanopillar still has obvious streak-like defects, and there is a reduction of nanopins in the nanopillar gap. When the thickness of the copper film is 24 nm, the quality of the prepared nanopillar array is relatively higher, with fewer stripes on the sidewalls of the nanopillars, reduced roughness, and fewer nanoneedles in the gaps of the nanopillars. With the longer deposition time of the copper film, the etching resistance of the mask increases. However, a certain thickness of the copper film is also sputtered into the gaps between the PS spheres, resulting in a certain etching resistance in the nanopillar gaps, which affects the further increase in nanopillar height. The average heights of the nanopillars prepared by etching were 218, 200, 221, 190, 145, and 152 nm for copper film thicknesses of 8, 16, 24, 32, 40, and 48 nm, respectively. Taking into account the height and roughness of diamond nanopillars prepared under copper etching mask layers of different thicknesses, the copper film with a thickness of 24 nm was chosen as the antietching layer for the PS spheres.

On the basis of the PS ball array film with an average diameter of 408 nm, as shown in Figure 3h, a 24 nm-thick Cu film was deposited to increase the etching resistance of the PS balls, and the effect of each parameter on the etching quality of the diamond nanopillars was explored by changing the parameters of the oxygen etching process. Compared to Figure 5a–c, under the conditions of a bias power of 50 W and

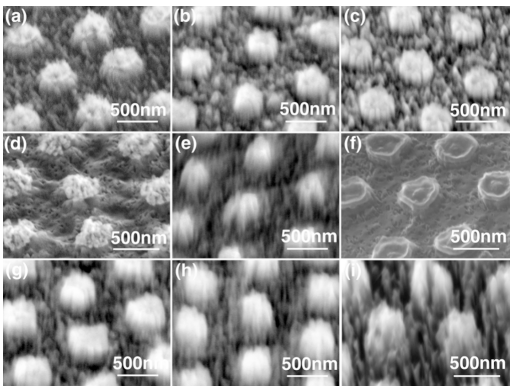

Figure 5. Diamond nanopillars with different etching parameters. The etching power, bias power, and etching time are (a) 200 W, 50 W, and 10 min, (b) 300 W, 50 W, and 10 min, (c) 400 W, 50 W, and 10 min, (d) 300 W, 20 W, and 10 min, (e) 300 W, 80 W, and 10 min, (f) 300 W, 50 W, and 5 min, (g) 300 W, 50 W, and 15 min, (h) 300 W, 50 W, and 20 min, and (i) 300 W, 50 W, and 40 min.

an etching time of 10 min, the structure of the nanopillar array remains unchanged at different etching powers (200, 300, and 400 W). The nanopillar spacing is maintained at around 800 nm, consistent with that of the PS sphere monolayer film. As the etching power increases, the nanopillar diameter decreases, measuring 446, 382, and 365 nm, respectively. Higher etching power leads to more severe etching of the copper etch-resistant layer. Additionally, with the increase in etching power, the sidewalls of the nanopillars gradually become rougher, exhibiting striped grooves on the surface and an increase in nanoneedles at the nanopillar gaps (as it can be seen in SEM images).

Comparing Figure 5b,d,e, under the constant conditions of an etching power at 300 W and an etching time of 10 min, the verticality of diamond nanopillar sidewalls gradually increases with the increase in bias power. At bias powers of 20, 50, and 80 W, the angles between the sidewalls and the vertical are 55°, 10°, and 7° respectively. Moreover, as the bias power increases, the etching effect on diamond gradually intensifies. When the bias power reaches 80 W, the nanopillars are noticeably damaged, and the number of nanoneedles at the gaps between nanopillars increases. Comparing with Figure 5b,f–i, keeping the etching power of 300 W and the bias power of 50 W unchanged, the structure of the nanopillar arrays remains intact under different etching times (5, 10, 15, 20, and 40 min), with an average diameter of 404 nm and a spacing of 800 nm, and the etching time mainly affects the height of diamond nanopillars, with the longer the etching time, the higher the nanopillars are. The nanopillar heights under the etching times of 5, 10, 15, 20, and 40 min were 132, 230, 281, 360, and 574 nm, respectively (measurements can be obtained from the SEM images). The increase in nanopillar height with etching time did not show a linear trend, which may be due to the consumption of the etch-resistant Cu film during the etching process.

The nanopillar arrays, prepared with an etching power of 300 W, a bias power of 50 W, and an etching time of 40 min, were examined using an atomic force microscope. As depicted in Figure 6a, the sidewalls of the nanopillars display distinct grooved stripes, while each nanopillar's frontal surface presents a petal-like structure. The measurements indicate surface arithmetic mean deviation (Ra) values of approximately 10 nm

https://doi.org/10.1021/acsomega.4c02618
ACS Omega 2024, 9, 27492–27498

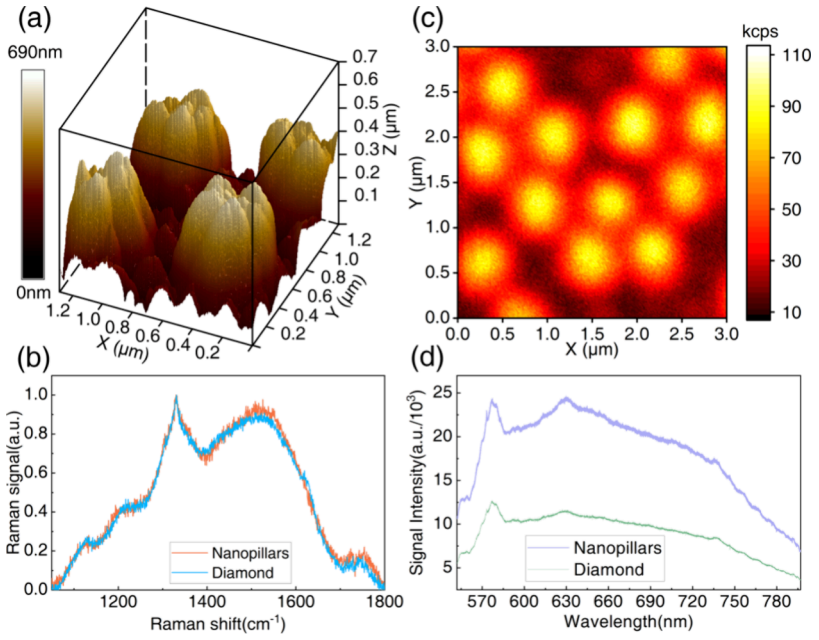

Figure 6. Performance testing of diamond nanopillar arrays: (a) AFM detection, (b) Raman spectroscopy, (c) fluorescence scanning, and (d) fluorescence spectroscopy.

on the frontal surface of the nanopillars and approximately 25 nm on the surfaces of the nanopillar gaps. Using Raman fluorescence coherent confocal microscopy, Raman and fluorescence spectroscopy was performed on both diamond films and diamond nanopillar arrays. Figure 6b depicts the Raman spectra of diamond films and diamond nanopillar arrays. For comparison purposes, the Raman spectra were deconvoluted and analyzed using Gaussian profiles and background subtraction, with normalization performed using the peak value at 1332 cm^{-1} for the diamond Raman peak. In the Raman spectra, the peaks at 1120, 1210, and 1430 cm^{-1} are associated with the vibrational modes of *trans*-polyacetylene (*trans*-PA).[33,34] The D-band near 1330 cm^{-1} indicates the "breathing" vibration mode of sp^2-bonded carbon atoms in rings.[35] Additionally, the peak at 1545 cm^{-1} corresponding to the graphite G-band is attributed to the in-plane stretching mode of sp^2-bonded carbon atoms in chains and rings.[36] The peak at 1750 cm^{-1} is attributed to the characteristics of sp^2 hybridization (chains or isolated clusters).[34] After the preparation of diamond nanopillar arrays, the diamond Raman spectra remain essentially unchanged, indicating that the prepared diamond nanopillars still exhibit polycrystalline diamond properties. Upon comparison, there is a slight increase in the graphite phase G peak, which may be attributed to residual graphite on the surface of the nanopillars during the etching process.

Using a confocal microscopy system, the luminescence intensity at various positions of the nanopillar array structure was detected, as illustrated in Figure 6c. Within a detection area of 3 μm × 3 μm, regularly arranged light spots were observed, with an approximate spacing of 800 nm, consistent with the dimensions of the fabricated nanopillar array structures. Taking into account the limitations set by the objective's collection angle and the diffraction limit of the laser spot, fluorescence spectra were separately measured for the diamond color centers on the large-area array of nanopillar structures and on the regions of the same sample surface where nanopillars were not fabricated for the purpose of comparison.

Figure 6d illustrates the fluorescence spectra of diamond films and diamond nanopillar arrays. Due to the inevitable presence of nitrogen sources in the preparation gas, nitrogen vacancy (NV) centers exist in diamond, exhibiting NV^0 and NV^- color center emission peaks near 575 and 637 nm, respectively, with a weak SiV^- color center emission peak around 738 nm, possibly introduced by plasma etching of the silicon substrate and glass observation windows of the equipment during diamond growth. By comparing the spectral intensities before and after preparing the nanopillar array, the photoluminescence intensities of NV^0, NV^-, and SiV^- color centers increased by 1.9, 2.1, and 2 times, respectively, indicating that preparing diamond nanopillar arrays can enhance the fluorescence of diamond color centers.

4. CONCLUSIONS

In this paper, tightly arranged PS ball array films were prepared on the diamond surface by the gas−liquid interface method, the controlled reduction of PS ball diameter was realized by the oxygen plasma etching process, a certain thickness of the copper film was sputtered on the surface of the reduced PS ball arrays by the tilted magnetron sputtering method to increase the etching resistance, and finally, diamond nanopillar arrays were prepared under the array mask by oxygen plasma etching. PS sphere array membrane preparation was found in which ethanol could promote the agglomeration of PS spheres and an SDS solution could make the agglomerated PS spheres tightly aligned. In the array mask preparation, it is found that the etching power can control the surface roughness of PS spheres, the bias power can control the shrinkage rate of PS spheres, and the Cu film plays a key role in the antietching ability of PS spheres, but Cu, if it is too thick, will affect the etching of the nanopillar gap. The prepared diamond nanopillar arrays were hexagonal dense row arrays with an average diameter of 404 nm and a spacing of 800 nm. The etching power can control the surface roughness of the nanopillar, the bias power can control the verticality of the nanopillar, and the etching time can control the height of the nanopillar. When the etching time

https://doi.org/10.1021/acsomega.4c02618
ACS Omega 2024, 9, 27492−27498

is 40 min, the height of the nanopillar is 574 nm. Raman spectroscopy and photoluminescence spectroscopy detection revealed that the prepared diamond nanopillar array still maintains polycrystalline diamond properties, with only a small amount of graphite phase appearing. Moreover, the prepared diamond nanopillar array can enhance the photoluminescence of diamond color centers by approximately 2 times. The fabrication method of diamond nanopillar array structures described in this paper lays the foundation for quantum sensing technology based on diamond nanostructures.

AUTHOR INFORMATION

Corresponding Author

Xin Tan − *School of Mechanical Engineering, Inner Mongolia University of Science & Technology, Baotou PR 014010, China; Inner Mongolia Key Laboratory of Intelligent Diagnosis and Control of Mechatronic System, Baotou PR 014010, China; Inner Mongolia University of Science and Technology Key Laboratory of Micro-Nano Structure Design and Manufacturing Technology, Baotou PR 014010, China;* orcid.org/0000-0001-8314-8032; Email: heart_tan@126.com

Authors

Zhanqing He − *School of Mechanical Engineering, Inner Mongolia University of Science & Technology, Baotou PR 014010, China*

Wenbin Li − *School of Mechanical Engineering, Inner Mongolia University of Science & Technology, Baotou PR 014010, China*

Qiao Yang − *School of Mechanical Engineering, Inner Mongolia University of Science & Technology, Baotou PR 014010, China*

Jian Wang − *School of Mechanical Engineering, Inner Mongolia University of Science & Technology, Baotou PR 014010, China*

Lei Cang − *School of Mechanical Engineering, Inner Mongolia University of Science & Technology, Baotou PR 014010, China*

Yanlong Du − *School of Mechanical Engineering, Inner Mongolia University of Science & Technology, Baotou PR 014010, China*

Hui Qi − *School of Mechanical Engineering, Inner Mongolia University of Science & Technology, Baotou PR 014010, China*

Complete contact information is available at: https://pubs.acs.org/10.1021/acsomega.4c02618

Author Contributions

The manuscript was written through contributions of all authors. All authors have given approval to the final version of the manuscript.

Notes

The authors declare no competing financial interest.

ACKNOWLEDGMENTS

We acknowledge support from the National Natural Science Foundation of China (62365015, 61765012, and 51965053), the Natural Science Foundation of Inner Mongolia (2023MS05047, 2019MS05008, and 2020MS05036), the Fundamental Research Funds for Inner Mongolia University of Science & Technology (2023RCTD011 and 2023YXXS012), the National Key Research and Development Program of China (2017YFF0207200 and 2017YFF0207203), the Research Program of Science and Technology at Universities of Inner Mongolia Autonomous Region (2017CXYD-2 and KCBJ2018031), the Inner Mongolia University of Science and Technology Youth Fund Project (202/0303022006), and the Scientific Research Program of Higher Education Institutions in Inner Mongolia Autonomous Region (NJZY23082).

REFERENCES

(1) Hanlon, L.; Gautam, V.; Wood, J. D. A.; et al. Diamond nanopillar arrays for quantum microscopy of neuronal signals. *Neurophotonics* **2020**, *7* (3), No. 035002.

(2) Zhu, T. Q.; Rhensius, J.; Herb, K.; et al. Multicone Diamond Waveguides for Nanoscale Quantum Sensing[J]. *Nano Lett.* **2023**, *23* (22), 10110−10117.

(3) Ali Momenzadeh, S.; Stöhr, R. J.; Favaro de Oliveira, F.; et al. Nanoengineered Diamond Waveguide as a Robust Bright Platform for Nanomagnetometry Using Shallow Nitrogen Vacancy Centers. *Nano Lett.* **2014**, *15* (1), 165−169.

(4) Maletinsky, P.; Hong, S.; Grinolds, M. S.; Hausmann, B.; et al. A robust scanning diamond sensor for nanoscale imaging with single nitrogen-vacancy centres. *Nat. Nanotechnol.* **2017**, *7* (5), 320−324.

(5) Riedrich-Möller, J.; Arend, C.; Pauly, C.; et al. Deterministic Coupling of a Single Silicon-Vacancy Color Center to a Photonic Crystal Cavity in Diamond. *Nano Lett.* **2014**, *14* (9), 5281.

(6) Radulaski, M.; Widmann, M.; Niethammer, M.; et al. Scalable quantum photonics with single color centers in silicon carbide[J]. *Nano. Letts* **2017**, *17* (3), 1782−1786.

(7) Pingault, H. B.; Becker, J. N.; Schulte, C. H. H.; et al. All-optical formation of coherent dark states of silicon-vacancy spins in diamond[J]. *Phys. Rev. Lett.* **2014**, *113* (26), No. 263601.

(8) Wang, H.; Duan, Z. C.; Li, Y. H.; et al. Near-Transform-Limited Single Photons from an Efficient Solid-State Quantum Emitter[J]. *Physical RevieW Letters* **2016**, *116* (21), No. 213601.

(9) McCloskey, D. J.; David, A.; et al. Enhanced Widefield Quantum Sensing with Nitrogen-Vacancy Ensembles Using Diamond Nanopillar Arrays. *ACS Appl. Mater. Interfaces* **2020**, *12* (11), 13421−13427.

(10) Guo, M.; Liu, P.; Huang, B. X.; et al. Hierarchical assembly of silver and gold nanoparticles in two-dimension: Toward fluorescence enhanced detection platforms[J]. *Appl. Surf. Sci.* **2019**, *476*, 1072−1078.

(11) Yin, J.; Zang, Y. S.; Yue, C.; et al. Multiple coupling in plasmonic metal/dielectric hollow nanocavity arrays for highly sensitive detection[J]. *Nanoscale* **2015**, *7* (32), 13495−13502.

(12) Kelaita, Y. A.; Fischer, K. A.; Babinec, T. M.; et al. Hybrid metal-dielectric nanocavity for enhanced light-matter interactions. *Opt. Mater. Express* **2017**, *7* (1), 000231.

(13) Babinec, T. M.; Hausmann, B. J.; Khan, M.; Zhang, Y.; et al. A diamond nanowire single-photon source[J]. *Nat. Nanotechnol* **2010**, *5*, 195−199.

(14) Masuda, H.; Yanagishita, T.; Yasui, K.; et al. Synthesis of Well-Aligned Diamond Nanocylinders[J]. *Adv. Mater.* **2001**, *13* (4), 247−249.

(15) Wang, C. F.; Hanson, R.; Awschalom, D. D.; et al. Fabrication and characterization of two-dimensional photonic crystal microcavities in nanocrystalline diamond. *Appl. Phys. Lett.* **2007**, *91* (20), 201112.

(16) Tsarik, K. A. Focused-Ion-Beam Exposure of an Ultrathin Electron-Beam Resist for the Formation of Nanoscale Field-Effect Transistor Contacts. Semiconductors. *Semiconductors* **2022**, *56*, 444−449, DOI: 10.1134/S1063782622130139.

(17) Losero, E.; Jagannath, S.; Pezzoli, M.; et al. Neuronal growth on high-aspect-ratio diamond nanopillar arrays for biosensing applications. *Sci. Rep.* **2023**, *13* (1), 5909.

(18) Schmidt, A.; Bernardoff, J.; Singer, K.; et al. Fabrication of Nanopillars on Nanocrystalline Diamond Membranes for the Incorporation of Color Centers. *Phys. Status Solidi A* **2019**, *216* (21), 1900233.
(19) Mehedi, H.; Mille, V.; Achard, J.; et al. Effect of the process parameters of inductively coupled plasma reactive ion etching on the fabrication of diamond nanotips. *Phys. Status Solidi A* **2014**, *211* (10), 2343−2346.
(20) Kunuku, S.; Sankaran, K. J.; Tsai, C. Y.; et al. Investigations on Diamond Nanostructuring of Different Morphologies by the Reactive-Ion Etching Process and Their Potential Applications[J]. *Acs Appl. Mater. Interfaces* **2013**, *5* (15), 7439−7449.
(21) Domonkos, M.; Jackivová, R.; Pathó, A. Image analysis algorithm for the verification of hexagonal symmetry in spherical nanostructures. *Microelectron. Eng.* **2022**, *251*, No. 111635.
(22) Domonkos, M.; Ižák, T.; Stolcova, L.; et al. Fabrication of periodically ordered diamond nanostructures by microsphere lithography. *Phys. Status Solidi B* **2014**, *251* (12), 2587−2592.
(23) Li, C. Y.; Hatta, A. Effect of metal coating on the formation of diamond Whiskers in O 2 RF plasma[J]. *Diamond & Related Materials* **2006**, *15* (2), 357−360.
(24) Babchenko, O.; Kromka, A.; Hruska, K.; et al. Nanostructuring of diamond films using self-assembled nanoparticles. *Open Phys.* **2009**, *7* (2), 310−314.
(25) Smirnov, W.; Kriele, A.; Yang, N.; Nebel, C. E. Aligned diamond nano-Wires: Fabrication and characterisation for advanced applications in bio- and electrochemistry[J]. *Diamond & Related Materials* **2010**, *19* (2), 186−189.
(26) Janssen, W.; Gheeraert, E. Dry etching of diamond nanowires using self-organized metal droplet masks. *Diamond Relat. Mater.* **2011**, *20* (3), 389−394.
(27) Domonkos, M.; Kromka, A. Nanosphere Lithography-Based Fabrication of Spherical Nanostructures and Verification of Their Hexagonal Symmetries by Image Analysis. *Symmetry* **2022**, *14*, 2642.
(28) Tan, X.; He, Z.; Yang, Q.; et al. Controllable preparation of single-crystal diamond nanopillar clusters by metal cyclic dewetting process. *Appl. Surf. Sci.* **2023**, *609*, No. 155246.
(29) Domonkos, M.; Ižák, T.; Varga, M.; et al. Diamond nucleation and growth on horizontally and vertically aligned Si substrates at low pressure in a linear antenna microwave plasma system. *Diamond Relat. Mater.* **2018**, *82*, 41−49.
(30) Janssen, W.; Gheeraert, E. Dry etching of diamond nanowires using self-organized metal droplet masks. *Diamond Relat. Mater.* **2011**, *20*, 389−39.
(31) Domonkos, M.; Ižák, T.; Štolcová, L.et al.Controlled Structuring of Self-assembled Polystyrene Microsphere Arrays by Two Different Plasma Systems. In *Proceedings of the 5th International Conference NanoCon, Brno*, Czech Republic, 2013, *10*, 1618
(32) Domonkos, M.; Demo, P.; Kromka, A. Nanosphere Lithography for Structuring Polycrystalline Diamond Films. *Crystals* **2020**, *10* (2), 118.
(33) Ferrari, A. C.; Robertson, J. Resonant Raman spectroscopy of disordered, amorphous, and diamondlike carbon[J]. *Phys. Rev. B* **2001**, *64*, No. 075414.
(34) Ferrari, A. C.; Robertson, J. Interpretation of Raman spectra of disordered and amorphous carbon[J]. *Phys. Rev. B* **2000**, *61*, 14095−14107.
(35) Klauser, F.; Steinmüller-Nethl, D.; Kaindl, R.; et al. Raman Studies of Nano- and Ultra-nanocrystalline Diamond Films Grown by Hot-Filament CVD[J]. *Chem. Vap. Deposition.* **2010**, *16*, 127−135.
(36) Vlasov, I. I.; Goovaerts, E.; Ralchenko, V. G.; et al. Vibrational properties of nitrogen-doped ultrananocrystalline diamond films grown by microwave plasma CVD[J]. *Diam. Relat. Mater.* **2007**, *16*, 2074−2077.

https://doi.org/10.1021/acsomega.4c02618
ACS Omega 2024, 9, 27492−27498